



Published in final edited form as:

*Nanomedicine*. 2012 July ; 8(5): 731–739. doi:10.1016/j.nano.2011.08.014.

## Enhanced delivery of $\alpha$ -glucosidase for Pompe disease by ICAM-1-targeted nanocarriers: comparative performance of a strategy for three distinct lysosomal storage disorders

Janet Hsu, B.S.<sup>1</sup>, Laura Northrup, B.S.<sup>2</sup>, Tridib Bhowmick, Ph.D.<sup>3</sup>, and Silvia Muro, Ph.D.<sup>1,3,\*</sup>

<sup>1</sup>Fischell Department of Bioengineering, School of Engineering, University of Maryland, College Park, MD 20742, USA

<sup>2</sup>Molecular and Cellular Bioengineering Research Experiences for Undergraduates, University of Maryland, College Park, MD 20742, USA

<sup>3</sup>Institute for Bioscience and Biotechnology Research, University of Maryland, College Park, MD 20742, USA

### Abstract

Enzyme replacement therapies for lysosomal storage disorders are often hindered by suboptimal biodistribution of recombinant enzymes after systemic injection. This is the case for Pompe disease caused by acid  $\alpha$ -glucosidase (GAA) deficiency, leading to excess glycogen storage through the body, mainly the liver and striated muscle. Targeting intercellular adhesion molecule-1 (ICAM-1), a protein involved in inflammation and overexpressed on most cells under pathological conditions, provides broad biodistribution and lysosomal transport of therapeutic cargoes. To improve its delivery, we coupled GAA to polymer nanocarriers (~180-nm) coated with anti-ICAM. Fluorescence microscopy showed specific targeting of anti-ICAM/GAA NCs to cells, with efficient internalization and lysosomal transport, enhancing glycogen degradation over non-targeted GAA. Radioisotope tracing in mice demonstrated enhanced GAA accumulation in all organs, including Pompe targets. Along with improved delivery of Niemann-Pick and Fabry enzymes, previously described, these results indicate that ICAM-1 targeting holds promise as a broad platform for lysosomal enzyme delivery.

### Keywords

ICAM-1; polymer nanocarriers; lysosomal storage disorders; enzyme replacement therapy;  $\alpha$ -glucosidase

---

© 2011 Elsevier Inc. All rights reserved.

\*Address correspondence to: Silvia Muro, 5115 Plant Sciences Building, College Park, MD 20742-4450. Tel. 1+301-405-4777; Fax. 1+301-314-9075; muro@umd.edu.

The authors do not have any competing interests to disclose.

**Publisher's Disclaimer:** This is a PDF file of an unedited manuscript that has been accepted for publication. As a service to our customers we are providing this early version of the manuscript. The manuscript will undergo copyediting, typesetting, and review of the resulting proof before it is published in its final citable form. Please note that during the production process errors may be discovered which could affect the content, and all legal disclaimers that apply to the journal pertain.

## BACKGROUND

The lysosomal storage disorders (LSDs) are inherited diseases often due to deficiency of lysosomal enzymes.<sup>1</sup> This is the case for Pompe disease caused by deficiency of acid  $\alpha$ -glucosidase (GAA, an enzyme that hydrolyzes glycogen to glucose), which results in aberrant glycogen storage within lysosomes.<sup>2</sup> Given that the liver and striated (cardiac and skeletal) muscle are more dependent on GAA activity, Pompe disease markedly affects these tissues.<sup>2-4</sup> In addition, Pompe disease manifests in other organs, including the nervous system and the vasculature.<sup>2</sup> Therefore, therapeutic intervention of this disease requires correction of GAA deficiency throughout the body, with emphasis on the liver and striated muscle.

Current treatment for Pompe disease utilizes enzyme replacement therapy (ERT), which substitutes deficient human GAA with a recombinant counterpart.<sup>5-8</sup> Recombinant GAA is glycosylated and can bind to mannose-6-phosphate receptors (M6PRs) on cells, which results in clathrin-dependent endocytosis and transport to lysosomes.<sup>9,10</sup> Systemic infusion of GAA reduces heart accumulation of glycogen, yet treatment of skeletal muscle and other tissues remain challenging.<sup>8,11</sup> Poor access of recombinant GAA to these tissues, altered M6PR expression in LSDs, and/or antibody production against the injected enzyme reduces response to therapy.<sup>12-17</sup> Although ERT efficacy can be enhanced by immunomodulators, this poses considerable risk,<sup>18-20</sup> emphasizing the need for alternative therapeutic options.

An experimental strategy that enhances delivery of other lysosomal enzymes is that of coupling said enzymes to polymer nanocarriers targeted to intercellular adhesion molecule (ICAM-1).<sup>21-25</sup> ICAM-1 is a transmembrane protein functionally involved in inflammation.<sup>26,27</sup> It is present on endothelial and other cell types, and is over-expressed in many inflammatory pathologies, including LSDs.<sup>26,27</sup> Binding of anti-ICAM nanocarriers to ICAM-1 results in carrier endocytosis by cells and transport to lysosomes.<sup>28,29</sup> This strategy is expected to provide broad distribution of therapeutics through the body, most favorably to disease sites), and lysosomal delivery, amenable for LSD treatment.

Previous works have shown that polymer nanoparticles (100–200 nm in diameter) coated with anti-ICAM enhance delivery of lysosomal enzymes in cell cultures and mice, bypass clathrin-mediated endocytosis of these enzymes, and provide marked attenuation of aberrant lysosomal storage.<sup>22,24,25</sup> Yet, the biodistribution pattern of anti-ICAM nanocarriers (anti-ICAM NCs) is slightly different depending on cargo.<sup>21,22</sup> Also, the nature of the substrate storage of each LSD and the resulting dysfunction impacts endocytosis and intracellular trafficking,<sup>12,14,30,31</sup> possibly affecting the delivery efficiency in particular disease settings. Whether the potential of ICAM-1-targeting strategy stands in other LSDs is an open question, e.g., accumulation of anti-ICAM NCs in skeletal muscle (a Pompe disease target) has never been tested.

In this work we have used fluorescence microscopy and radioisotope tracing to evaluate anti-ICAM/GAA NC binding, internalization, lysosomal transport, and attenuation of the excess glycogen storage in cell cultures, as well as biodistribution in mice, showing the potential of this strategy in the context of Pompe disease. We have also compared anti-ICAM/GAA NCs to formulations carrying other lysosomal enzymes to estimate the potential of the ICAM-1-targeting strategy as a broad enzyme delivery platform for LSDs.

## METHODS

### Antibodies and reagents

Monoclonal antibodies to human or murine ICAM-1 (anti-ICAM) were R6.5<sup>26</sup> or YN1.<sup>32</sup> Secondary antibodies were from Jackson ImmunoResearch (West Grove, PA, USA). *Saccharomyces cerevisiae* recombinant  $\alpha$ -glucosidase (GAA) was from Sigma Aldrich (St. Louis, MO, USA). Polystyrene beads (100 nm-diameter) were from Polysciences (Warrington, PA, USA). Cell culture reagents were from Cellgro (Manassas, VA, USA) or Gibco BRL (Grand Island, NY, USA). Other reagents were from Sigma Aldrich.

### Preparation of anti-ICAM/GAA nanocarriers and enzyme release

Model polymer nanocarriers were prepared by coating 100 nm-diameter polystyrene beads by surface adsorption with anti-ICAM (anti-ICAM NCs) or a mix of anti-ICAM and GAA (anti-ICAM/GAA NCs).<sup>22</sup> A 95:5 antibody:enzyme mass ratio was used *in vivo*, as minimal amounts of GAA are needed to trace its biodistribution, and a 50:50 mass ratio was used in cell cultures to obtain measurable effects. FITC particles were used for fluorescence microscopy. Alternatively, 5% of total GAA was labeled with <sup>125</sup>Iodine (<sup>125</sup>I-GAA). After coating, nanocarriers were washed and centrifuged to remove free anti-ICAM and GAA, resuspended in 1% bovine serum albumin (BSA) and sonicated to avoid aggregation. This protocol rendered ~180±7 nm particles (0.2 polydispersity) by dynamic light scattering (Zetasizer Nano-ZS90; Malvern Instruments Inc., Westborough, MA). This is a prototype not intended for clinical use, yet a valid model to demonstrate targeting since these particles display similar coating efficacy, targeting, and intracellular transport<sup>21,33</sup> as anti-ICAM NCs made of poly(lactic-co-glycolic acid),<sup>34,35</sup> a material approved by the US Food and Drug Administration. The nanocarrier concentrations used were estimated from the literature to display enough radioisotope tracing and biochemical effects.<sup>6,7,21,22</sup>

Release of <sup>125</sup>I-GAA from anti-ICAM NCs was determined by centrifugation to separate free enzyme from particle-bound fraction.<sup>23</sup> Mechanical GAA release was determined after centrifugation, resuspension by pipetting, and sonication. Enzyme release was tested after incubation in storage buffer (phosphate buffer saline, PBS, supplemented with 1% bovine serum albumin, BSA) or complete cell medium (described below), at 4°C or 37°C, pH 7.4 or pH 4.5, and in the absence or presence of 50mg/mL glycogen, the enzyme substrate.

### Cell cultures

Endothelial cells represent the first cell layer encountered by injected lysosomal enzymes and targeting these cells impacts organ accumulation. We used human umbilical vein endothelial cells (HUVECs; Clonetics, San Diego, CA, USA) maintained in M-199 supplemented as described,<sup>22</sup> and seeded on 1% gelatin-coated coverslips. Skeletal muscle cells were isolated from C57Bl/6 mouse gastrocnemius and quadriceps by digestion with 0.2 mg/mL collagenase for 24 hours at 37°C, and seeded on matrigel (BD Biosciences, Franklin Lakes, NJ, USA). Cells were activated overnight with 10 ng/mL tumor necrosis factor- $\alpha$  (TNF- $\alpha$ ; BD Biosciences, Franklin Lakes, NJ, USA), to up-regulate ICAM-1 expression as in pathology.<sup>22,26,27</sup>

Pompe disease-model cells were generated by treating cells overnight with 300 or 600  $\mu$ M D(+)-turanose, a GAA competitive inhibitor.<sup>2,36</sup> Glycogen accumulation was verified by staining fixed cells with periodic acid-Schiff (PAS).<sup>37</sup> Semi-quantitative measurement of glycogen was assessed using an Olympus IX81 microscope (Olympus, Inc., Center Valley, PA) with a 40X objective (UPlanApo, Olympus, Inc.). Bright field micrographs were captured under blue, green and red filters (1160A-OMF, 3540B-OMF, 4040B-OMF; Semrock, Inc., Rochester, NY) with an ORCA-ER camera (Hamamatsu Corporation,

Bridgewater, NJ) and combined them with SlideBook™ 4.2 (Intelligent Imaging Innovations, Inc., Denver, CO). Red glycogen was quantified with Image-Pro 6.3 (Media Cybernetics, Inc., Bethesda, MD) and normalized per cell.

### Binding, internalization and lysosomal co-localization of anti-ICAM/GAA nanocarriers

Control cells or Pompe disease-model cells were incubated at 37°C with FITC anti-ICAM NCs or anti-ICAM/GAA NCs (2.5 µg GAA/mL, 7×10<sup>10</sup> particles/mL) for 30 min to allow binding. Cells were left undisturbed or washed to remove unbound nanocarriers (pulse-chase incubation to synchronize transport) for a total time of 1 h or 3 h, to determine endocytosis. Alternatively, 3 mM amiloride (inhibitor of CAM endocytosis) or 50 µM monodansylcadaverine (MDC) (inhibitor of clathrin endocytosis) were used.<sup>28</sup> Cells were washed, fixed and surface-bound carriers were stained using Texas-Red goat anti-mouse IgG that recognizes anti-ICAM on particles located on the cell surface (yellow color) but cannot access those endocytosed by the cell (green color).<sup>28</sup> The nucleus was stained with blue DAPI. Fluorescence microscopy was used to determine the percentage of nanocarriers internalized per cell.<sup>28</sup>

To examine intracellular transport of nanocarriers, lysosomes were labeled by incubating cells with Texas-Red dextran (1.5 h, 37C), followed by washing and 1 h incubation with FITC anti-ICAM/GAA NCs.<sup>29</sup> Cells were then washed and fixed, or incubated for 2 h or 4 h more to synchronize intracellular transport of carriers.<sup>29</sup> Co-localization of green fluorescent nanocarriers with red-labeled lysosomes (yellow color) was analyzed by fluorescence microscopy.<sup>29</sup>

### Glycogen degradation by anti-ICAM/GAA nanocarriers

Pompe disease-model cells were incubated at 37°C for 5 h with anti-ICAM/GAA NCs or non-targeted GAA (2.5 µg/ml GAA), in the presence of 300 µM chloroquine.<sup>22</sup> Chloroquine is used because removal of turanose (required to avoid inhibition of the delivered GAA) may render endogenous GAA active. Chloroquine neutralizes lysosomes and inhibits endogenous lysosomal enzymes that have acidic pKa without affecting the exogenous neutral GAA. After incubation, samples were fixed, stained with PAS, and analyzed by microscopy to quantify glycogen degradation as follows:

$$\% \text{ Glycogen degradation} = 100 \times \left\{ 1 - \frac{(\text{Glycogen in diseased cells after treatment} - \text{Glycogen in control cells})}{(\text{Glycogen in diseased cells (without treatment)} - \text{Glycogen in control cells})} \right\}$$

### *In vivo* biodistribution

Anti-ICAM/<sup>125</sup>I-GAA NCs or free <sup>125</sup>I-GAA (51.4±3.7 µg/kg bodyweight) were injected intravenously into anesthetized C57BL/6 mice (Jackson Laboratory, Bar Harbor, ME, USA). Blood samples were collected at 2, 15, and 30 min. At 30 min, brain, heart, kidneys, liver, lungs, spleen, and left gastrocnemius and quadriceps muscles were collected. The radioactivity and weight of organs were used to calculate: (i) percentage of injected dose per organ (%ID) to compare the biodistribution of the injected formulations, (ii) percent injected dose per gram of organ (%ID/g) to compare relative distribution amongst organs of different sizes, (iii) localization ratio (LR; organ-to-blood ratio of %ID/g) to compare tissue-to-blood distribution, and (iv) specificity index (SI, targeted-to-untargeted LR ratio in a given organ) to compare efficiency of targeted to non-targeted formulation, as described.<sup>21,22</sup> Animal studies were performed following humane care guidelines and approved by IACUC.

## Statistics

Data were calculated as mean  $\pm$  standard error of the mean (SEM). Statistical significance was determined by unpaired Student's *t* tests.

## RESULTS

### Characterization of anti-ICAM/GAA nanocarriers and enzyme release

Anti-ICAM and GAA were coated onto 100 nm nanocarriers (anti-ICAM/GAA NCs). As shown in Table 1, the  $^{125}\text{I}$ -GAA loading efficiency was  $86.2\pm 4.3\%$ , rendering  $277.7\pm 1.4$  GAA molecules per carrier and diameter of  $180.1\pm 0.9$  nm when co-coated at a 50:50 mass ratio (selected based on the enzyme dose estimated to exert biochemical effects<sup>6,7</sup>).

The enzyme coat was stable through centrifugation, resuspension by pipetting, and sonication ( $11.6\pm 0.3\%$  enzyme release), and during storage at  $4^\circ\text{C}$  in buffer ( $0.0\pm 0.1\%$  to  $6.1\pm 0.5\%$  enzyme release within 3 days; Supplementary Figure 1). Incubation of anti-ICAM/ $^{125}\text{I}$ -GAA NCs at  $37^\circ\text{C}$  and neutral pH in complete cell medium also showed marked enzyme retention (e.g.,  $3.8\pm 0.2\%$  release at 3 h and  $11.9\pm 0.3\%$  release and 72 h). Enzyme release was markedly enhanced under conditions mimicking the lysosomal environment, e.g., pH 4.5 and presence of the enzyme substrate, glycogen ( $3.1$ ,  $7.9$ , and  $11.5$  fold increased compared to neutral pH at 30 min, 3 h, and 8 h, respectively).

### Targeting and internalization of anti-ICAM/GAA nanocarriers in Pompe disease-model cells

We generated Pompe disease-model cells by treating endothelial cells (the first layer of cells GAA encounters in the body after systemic administration) with turanose, a competitive inhibitor of GAA that induces glycogen accumulation.<sup>2</sup> As shown in Supplementary Figure 2, cells treated overnight with  $300\ \mu\text{M}$  turanose accumulated increased levels of glycogen over control cells, similar to some tissues from adult-onset Pompe disease patients.<sup>2,36</sup>

Targeting of anti-ICAM/GAA NCs in this model was assessed by fluorescence microscopy. As shown in Figure 1, *A* and Supplementary Figure 3, anti-ICAM/GAA NCs bound efficiently to cells:  $51.3\pm 4.7$  NCs/cell by 30 min and  $79.8\pm 8.3$  NCs/cell by 1 h, reaching a plateau. The level of binding of non-specific IgG NCs to control cells was  $2\pm 2$  NCs/cell (data not shown), demonstrating the specificity of anti-ICAM counterparts. Importantly, anti-ICAM NCs also bound to primary skeletal muscle cells (a major target in Pompe disease) isolated from mice (Figure 1, *B*). In these cells carriers seemed to align in the direction of cytoskeletal fibers, a feature previously observed during internalization of anti-ICAM NCs by endothelial cells.<sup>24,28</sup>

In agreement with this observation,  $78.6\pm 1.7\%$  of all bound anti-ICAM/GAA NCs were internalized by Pompe disease-model cells within the first 30 min (Figure 1, *C* and Supplementary Figure 4). Particle uptake slightly increased to  $85.0\pm 1.7\%$  and  $89.4\pm 0.4\%$  by 1 h and 3 h. This suggests efficient intracellular transport of GAA by anti-ICAM NCs ( $t_{1/2} = 10$  min) even in cells presenting aberrant glycogen storage, achieving almost complete uptake of nanocarriers that bind to the target.

In addition (Figure 1, *D* and Supplementary Figure 5) internalization of anti-ICAM/GAA NCs was inhibited by amiloride, a drug that affects cell adhesion molecule- (CAM)-mediated endocytosis ( $42.6\pm 1.6\%$  inhibition), but not MDC, an inhibitor of the clathrin-mediated pathway related to uptake of lysosomal enzymes ( $14.6\pm 1.0\%$  inhibition). This suggests that anti-ICAM NCs are capable of successfully shifting endocytosis of GAA from classical clathrin-coated pits to non-classical CAM-mediated pathway in a Pompe disease model.

## Lysosomal transport of anti-ICAM/GAA nanocarriers and reduction of glycogen storage in Pompe disease-model cells

We examined the intracellular trafficking of anti-ICAM/GAA NCs labeled with green FITC in Pompe disease-model cells whose lysosomes had been pre-labeled using Texas-Red dextran.<sup>29</sup> Fluorescence microscopy (Figure 2, *A*) showed a modest co-localization of green carriers with red lysosomes during the first hour ( $32.8 \pm 2.5\%$ ). However, delivery to lysosomes was significantly increased to  $63.6 \pm 2.2\%$  and  $77.3 \pm 2.8\%$  by 3 h and 5 h. This suggests that transport of the therapeutic cargo, GAA, to this compartment could be relatively efficient even in Pompe disease-model cells, supporting the potential of this strategy.

To confirm this, we measured glycogen reduction in Pompe disease model-cells after incubation with anti-ICAM/GAA NCs or a comparable amount of non-targeted GAA. After achieving aberrant glycogen storage in cells, turanose must be removed to avoid inhibition of the delivered enzyme. Hence, to ensure that glycogen attenuation was achieved by the exogenous neutral GAA after delivery, we inhibited the endogenous lysosomal acidic GAA by adding chloroquine to neutralize lysosomes. This strategy, used for  $\alpha$ -Gal delivery,<sup>22</sup> also mimics the lysosomal pH elevation observed in some LSDs,<sup>38</sup> including severe Pompe disease in which some cells exhibit a failure to lower the lysosomal pH below 6.0.<sup>14</sup>

As shown in Figure 2, *B*, glycogen degradation by anti-ICAM/GAA NCs was significantly enhanced (by  $\sim 3$  fold) compared to the same dose of non-targeted GAA ( $73.9 \pm 2.3\%$  versus  $26.0 \pm 0.9\%$  glycogen reduction, respectively), suggesting that lysosomal delivery achieved by anti-ICAM NCs may be therapeutically relevant as compared to the free enzyme counterpart.

## Biodistribution of anti-ICAM/GAA nanocarriers in mice

We then determined the *in vivo* biodistribution of anti-ICAM/<sup>125</sup>I-GAA NCs after intravenous administration in mice. Anti-ICAM/<sup>125</sup>I-GAA NCs rapidly disappeared from circulation, with only  $2.6 \pm 0.5\%$  of the injected dose (% ID) in blood by 1–2 min after injection, and remained low for the duration of the experiment (Supplementary Figure 6). This may be due to clearance from circulation and/or rapid targeting to ICAM-1-positive tissues. Indeed, we observed fast accumulation of anti-ICAM/<sup>125</sup>I-GAA NCs throughout the body (Figure 3, *A*, 30 min after injection). As expected, due to a first-pass effect of nanocarriers injected intravenously, its profuse vascularization, high ICAM-1 expression, and organ size, the lungs received the highest dose fraction ( $48.8 \pm 3.3\%$  ID). Liver accumulation followed ( $17.3 \pm 2.0\%$  ID), in accord with the size of this organ, its vascularization, high ICAM-1 expression and its role in blood clearance. Another organ of the reticulo-endothelial system, the spleen, accumulated a considerable fraction of anti-ICAM/<sup>125</sup>I-GAA NCs ( $2.9 \pm 0.3\%$  ID). Although more modest, nanocarriers were also found in the brain ( $0.15 \pm 0.01\%$  ID) and striated muscle: the heart received  $0.4 \pm 0.03\%$  ID and the gastrocnemius and quadriceps muscles accumulated  $0.07 \pm 0.01\%$  ID and  $0.08 \pm 0.01\%$  ID, respectively.

When the accumulation of anti-ICAM/<sup>125</sup>I-GAA NCs was normalized to respective tissue weight (% ID/g of organ; Figure 3, *B*), to compare organ specificity, the lungs remained the most heavily targeted organ with  $246.8 \pm 20.4\%$  ID/g. This was expected as the lungs contain 20–30% endothelium in the body with high ICAM-1 expression.<sup>21</sup> Next, high accumulation was found in the spleen ( $30.9 \pm 3.4\%$  ID/g), followed by the liver ( $12.8 \pm 1.6\%$  ID/g) and heart ( $2.9 \pm 0.2\%$  ID/g), and finally, skeletal muscle and brain:  $0.4 \pm 0.04\%$  ID/g and  $0.3 \pm 0.04\%$  ID/g in gastrocnemius and quadriceps muscles, and  $0.3 \pm 0.03\%$  ID/g in brain tissue.

## Comparative biodistribution of GAA delivered by anti-ICAM nanocarriers versus non-targeted GAA

We next compared the biodistribution of anti-ICAM/<sup>125</sup>I-GAA NCs to that of non-targeted <sup>125</sup>I-GAA (Figure 4). In contrast to anti-ICAM/<sup>125</sup>I-GAA NCs, free <sup>125</sup>I-GAA circulated significantly longer (e.g., 38.4±2.1 %ID at 30 min), suggesting lower affinity to tissues (Supplementary Figure 6). To correct for the difference in the circulating levels of <sup>125</sup>I-GAA versus anti-ICAM/<sup>125</sup>I-GAA NCs (~10 fold higher for non-targeted GAA), we calculated the localization ratio (LR; Figure 4, A). This parameter measures %ID of a formulation per gram of organ divided by %ID/g in blood (tissue-to-blood ratio).

Using this parameter, accumulation of ICAM-1-targeted <sup>125</sup>I-GAA in mouse organs significantly and consistently exceeded that of free <sup>125</sup>I-GAA, even in tissues which showed low levels of anti-ICAM/<sup>125</sup>I-GAA NCs. For example, in cardiac and skeletal muscle, anti-ICAM/<sup>125</sup>I-GAA NCs had LRs of 1.91±0.39, 0.31±0.05 and 0.25±0.03 for heart, gastrocnemius muscle and quadriceps muscle, versus non-targeted <sup>125</sup>I-GAA LRs of 0.17±0.01, 0.04±0.01 and 0.04±0.003. The specificity index (SI; Figure 4, B), which represents the LR ratio of targeted to non-targeted formulations, indicates that anti-ICAM NCs increased <sup>125</sup>I-GAA delivery to all organs: 584-fold increase in lungs, 67- in spleen, 23- in liver, 10- in heart, and 6-fold in skeletal muscle and brain, indicating great potential for anti-ICAM NCs to enhance GAA delivery *in vivo*.

## DISCUSSION

Our results indicate that ICAM-1-targeting holds potential to improve delivery of GAA for ERT of Pompe disease. Anti-ICAM/GAA NCs provided efficient targeting in Pompe disease-model cells and primary cultures of skeletal muscle, as well as internalization and lysosomal transport with attenuation of excess glycogen, surpassing the effects of free GAA. Anti-ICAM/GAA NCs also markedly enhanced enzyme delivery *in vivo* compared to non-targeted GAA in all tissues tested, including heart, skeletal muscle and liver, major targets in Pompe disease.

An adequate geometry of anti-ICAM carriers is crucial to modulate the efficacy of this strategy. Although cells in culture internalize anti-ICAM carriers within a wide range of geometries (~200 nm to 5 μm, spheres and elongated disks), sub-micrometer spherical carriers and micrometer elongated counterparts display more specific targeting *in vivo*, yet only sub-micrometer anti-ICAM NCs traffic efficiently to lysosomes.<sup>25</sup> Hence, sub-micrometer spherical anti-CAM carriers (shown in this work) display most adequate features for lysosomal enzyme delivery.

Using such geometry parameters, coating efficacy and stability of the <sup>125</sup>I-GAA coat on prototype anti-ICAM NCs under storage conditions and cell media were relatively high, while the enzyme was released under conditions mimicking the lysosomal microenvironment (Table 1 and Supplementary Figure 1), suitable for the intended application. Although our goal was to generate a prototype to prove targeting and biochemical effects, this configuration is still relevant since lysosomal enzymes are active at acidic lysosomal pH and act as pro-drugs prior to reaching this compartment. This loading capacity can translate into a dose of ~2 mg GAA/kg body weight, on the order of magnitude of current clinical doses of the non-targeted enzyme.<sup>7,8</sup>

Compared to nanocarriers coated at saturation with only anti-ICAM, GAA coating reduces the surface covered by antibody by ~50%. As described,<sup>39</sup> this is expected to reduce targeting. In agreement, our results show binding of ~80 NCs/cell after 1 h incubation (Figure 1, A, and Table 1), which is a ~50% reduction compared to anti-ICAM NCs (Table 1).

Nevertheless, binding was sufficient to target primary skeletal muscle cells (Figure 1, *B*), which express lower ICAM-1 levels than endothelial cells.<sup>27</sup> This binding surpassed by 35-fold targeting of control IgG NCs and provided sufficient delivery of GAA as to attenuate glycogen storage (Figure 2, *B*).

This outcome was possible due to relatively high efficiency of uptake of anti-ICAM/GAA NCs by cells: ~80% of all cell-bound carriers at 1h (Figure 1, *C*, and Table 1). The internalization rate and pathway were similar to that of anti-ICAM NCs (Table 1), despite differences in the binding of these formulations. This is in agreement with previous works showing efficient uptake of anti-ICAM NCs by cells regardless of their binding level.<sup>24,28</sup> Uptake is mediated by amiloride-sensitive CAM-mediated endocytosis, a pathway different from clathrin- and caveolar-mediated endocytosis, phagocytosis and macropinocytosis.<sup>24,28</sup>

Anti-ICAM/GAA NCs trafficked to lysosomes (e.g., 65% by 3 h), which was only minimally reduced compared to anti-ICAM NCs (75% by 3 h; Table 1). This could be due to the aberrant lysosomal storage in Pompe disease-model cells, which may affect transport, or the lower density of anti-ICAM on the carrier surface. Yet, lysosomal transport of anti-ICAM/GAA NC was sufficient to enhance glycogen degradation in Pompe-model cells by ~3 folds over non-targeted enzyme.

*In vivo* biodistribution of anti-ICAM/GAA NCs was also markedly enhanced in all tissues compared to non-targeted GAA (from ~5.5- to 580-fold; Figure 4, *B*). Main targets for Pompe disease, such as liver, heart and skeletal muscle, received ~23-, 11- and 6-fold increased GAA doses, demonstrating the efficacy of this strategy. This outcome is highly relevant since the liver represents a major storage compartment for glycogen, and the cardiac and skeletal muscles use glycogen as a source of energy.<sup>2</sup> This is the first time that ICAM-1 targeting is demonstrated for skeletal muscle (Figures 1, *B*, and 4, *B*), which may offer an avenue for drug delivery to this tissue. Enhanced GAA delivery to the brain (~6-fold) may attenuate neuropathology and cerebral vasculopathy observed in some patients.<sup>2</sup> Delivery to lungs, kidney, and spleen is also expected to be beneficial since these organs accumulate glycogen in GAA deficiency.<sup>2</sup> Hence, ICAM-1 targeting could represent an alternative or complementary strategy for ERT of Pompe disease. Although previous studies indicated no apparent toxicity of anti-ICAM NCs,<sup>21</sup> future studies will need to assess the biocompatibility of this approach.

This is the third example where ICAM-1-targeting shows a marked improvement, in cell culture and *in vivo*, in the context of LSD enzymes. Other examples include acid sphingomyelinase (ASM) deficient in types A-B Niemann-Pick disease<sup>40</sup> and  $\alpha$ -galactosidase ( $\alpha$ -Gal) deficient in Fabry disease.<sup>41</sup> The loading efficiency of these enzymes on anti-ICAM NCs was similar: 77 to 86% for anti-ICAM:enzyme 50:50 mass ratio formulations (Table 1). In all cases, this diminishes the density of anti-ICAM on the carrier by ~40–50% (Table 1). Although this results in a ~50% reduction in NC targeting for  $\alpha$ -Gal and GAA (in cell cultures), this effect is not observed for anti-ICAM/ASM NCs (Table 1). ASM on the NC surface may provide affinity to the cell surface, through binding to its substrate, sphingomyelin, abundantly present at the plasmalemma.<sup>30</sup>

In all cases, anti-ICAM/enzyme NC uptake was efficient: ~70–80% of cell bound NCs (Table 1), which occurred by CAM-mediated endocytosis (Figure 1, *D*, and <sup>22,25</sup>). This provided similarly efficient lysosomal delivery of ASM,  $\alpha$ -Gal and GAA (65–70%; Table 1), resulting in a substantial reduction of lysosomal storage of sphingomyelin, globotriaosylceramide and glycogen, substrates of these enzymes, respectively (Table 1). While 70–75% substrate reduction was observed for  $\alpha$ -Gal and GAA, ASM delivered by anti-ICAM NCs reduced substrate levels to control values, which may be due to

experimental differences: an acidic enzyme (ASM) was tested in genetic models<sup>24,25</sup> versus neutral  $\alpha$ -Gal22 and GAA tested in pharmacological models. In any instance, the enzymes delivered by anti-ICAM NCs improved substrate reduction by 2- to 3-fold compared to non-targeted counterparts (Table 1). These differences may be more acute *in vivo*, where binding of non-targeted enzymes may be further hindered due to blood flow.

Indeed, non-targeted ASM,  $\alpha$ -Gal and GAA accumulated more poorly than their anti-ICAM NC counterparts in all tissues in mice, including the brain and peripheral organs (SI, fold increase in the tissue-to-blood enzyme level when administered on nanocarriers; Table 2). In all cases, although brain accumulation was significantly improved by anti-ICAM NCs (~4–7 fold increase), this organ received the lowest dose compared to the lung and liver, which received the highest dose. First pass effect after intravenous injection and high ICAM-1 expression associated to the lung and liver may account for this pattern.

We observed some differences in tissue distribution of anti-ICAM NCs loaded with ASM,  $\alpha$ -Gal or GAA (Table 2). Anti-ICAM/ASM NCs provided the highest enhancement in brain delivery (7-fold), which is relevant since this organ is a more important target for type A Niemann-Pick disease.<sup>2,40,41</sup> Furthermore, despite lower density of targeting antibodies (Table 1), anti-ICAM/ASM NCs displayed greater brain accumulation than anti-ICAM NCs, perhaps due to ASM binding to abundant sphingomyelin in this organ. For an unknown reason, anti-ICAM/GAA provided the greatest affinity to the lungs (585 fold over GAA). This formulation also displayed higher accumulation in the heart (11 fold over GAA), which constitutes a very prevalent target for Pompe disease. This formulation also targeted the kidneys, liver and spleen at higher specificity compared to its non-targeted counterpart (9-, 23- and 67-fold over GAA).

Given that ultimately all tissues are affected at some degree by LSDs, and since anti-ICAM NCs enhances enzyme delivery to main targets of intervention in all three cases, ICAM-1-targeting strategy holds considerable promise as a general platform to improve ERT delivery for LSDs.

## Supplementary Material

Refer to Web version on PubMed Central for supplementary material.

## Acknowledgments

This work was supported by the NSF Research Experience for Undergraduates program of the Bioengineering Department in the University of Maryland (LN), Nanobiotechnology Program of the Maryland Department of Business and Economic Development, Minta Martin Foundation, AHA 09BGIA2450014, and R01HL098416 (SM).

The authors thank Edward Lim and Dave Dolak (Malvern Instruments Inc., Worcestershire, UK) for providing DLS size measurement of anti-ICAM/GAA NCs.

## References

1. Futerman AH, van Meer G. The cell biology of lysosomal storage disorders. *Nat Rev Mol Cell Biol.* 2004; 5:554–65. [PubMed: 15232573]
2. Hirschhorn, R.; Reuser, AJJ. Glycogen storage Disease Type II: Acid  $\alpha$ -Glucosidase (Acid Maltase) Deficiency. In: Scriver, C.; Beaudet, A.; Sly, W.; Valle, D.; Childs, B.; Kinzler, K., et al., editors. *The Metabolic and Molecular Bases of Inherited Disease.* 8. Vol. 3. New York: McGraw-Hill; 2001. p. 3389-420.

3. Malicdan MC, Noguchi S, Nonaka I, Saftig P, Nishino I. Lysosomal myopathies: an excessive build-up in autophagosomes is too much to handle. *Neuromuscul Disord.* 2008; 18:521–9. [PubMed: 18502640]
4. Shea L, Raben N. Autophagy in skeletal muscle: implications for Pompe disease. *Int J Clin Pharmacol Ther.* 2009; 47 (Suppl 1):S42–7. [PubMed: 20040311]
5. Burrow TA, Hopkin RJ, Leslie ND, Tinkle BT, Grabowski GA. Enzyme reconstitution/replacement therapy for lysosomal storage diseases. *Curr Opin Pediatr.* 2007; 19:628–35. [PubMed: 18025928]
6. Martiniuk F, Chen A, Donnabella V, Arvanitopoulos E, Slonim AE, Raben N, et al. Correction of glycogen storage disease type II by enzyme replacement with a recombinant human acid maltase produced by over-expression in a CHO-DHFR(neg) cell line. *Biochem Biophys Res Commun.* 2000; 276:917–23. [PubMed: 11027569]
7. Merk T, Wibmer T, Schumann C, Kruger S. Glycogen storage disease type II (Pompe disease)--influence of enzyme replacement therapy in adults. *Eur J Neurol.* 2009; 16:274–7. [PubMed: 19138339]
8. Schoser B, Hill V, Raben N. Therapeutic approaches in glycogen storage disease type II/Pompe Disease. *Neurotherapeutics.* 2008; 5:569–78. [PubMed: 19019308]
9. Neufeld EF. The uptake of enzymes into lysosomes: an overview. *Birth Defects Orig Artic Ser.* 1980; 16:77–84. [PubMed: 7448363]
10. Sly WS, Kaplan A, Achord DT, Brot FE, Bell CE. Receptor-mediated uptake of lysosomal enzymes. *Prog Clin Biol Res.* 1978; 23:547–51. [PubMed: 662919]
11. Fukuda T, Roberts A, Plotz PH, Raben N. Acid alpha-glucosidase deficiency (Pompe disease). *Curr Neurol Neurosci Rep.* 2007; 7:71–7. [PubMed: 17217857]
12. Cardone M, Porto C, Tarallo A, Vicinanza M, Rossi B, Polishchuk E, et al. Abnormal mannose-6-phosphate receptor trafficking impairs recombinant alpha-glucosidase uptake in Pompe disease fibroblasts. *Pathogenetics.* 2008; 1:6. [PubMed: 19046416]
13. de Vries JM, van der Beek NA, Kroos MA, Ozkan L, van Doorn PA, Richards SM, et al. High antibody titer in an adult with Pompe disease affects treatment with alglucosidase alfa. *Mol Genet Metab.* 2010; 101:338–45. [PubMed: 20826098]
14. Fukuda T, Ewan L, Bauer M, Mattaliano RJ, Zaal K, Ralston E, et al. Dysfunction of endocytic and autophagic pathways in a lysosomal storage disease. *Ann Neurol.* 2006; 59:700–8. [PubMed: 16532490]
15. Kishnani PS, Goldenberg PC, DeArme SL, Heller J, Benjamin D, Young S, et al. Cross-reactive immunologic material status affects treatment outcomes in Pompe disease infants. *Mol Genet Metab.* 2010; 99:26–33. [PubMed: 19775921]
16. Koeberl DD, Luo X, Sun B, McVie-Wylie A, Dai J, Li S, et al. Enhanced efficacy of enzyme replacement therapy in Pompe disease through mannose-6-phosphate receptor expression in skeletal muscle. *Mol Genet Metab.* 2011
17. Sun B, Li S, Bird A, Yi H, Kemper A, Thurberg BL, et al. Antibody formation and mannose-6-phosphate receptor expression impact the efficacy of muscle-specific transgene expression in murine Pompe disease. *J Gene Med.* 2010; 12:881–91. [PubMed: 20967919]
18. Joseph A, Munroe K, Housman M, Garman R, Richards S. Immune tolerance induction to enzyme-replacement therapy by co-administration of short-term, low-dose methotrexate in a murine Pompe disease model. *Clin Exp Immunol.* 2008; 152:138–46. [PubMed: 18307520]
19. Sun B, Bird A, Young SP, Kishnani PS, Chen YT, Koeberl DD. Enhanced response to enzyme replacement therapy in Pompe disease after the induction of immune tolerance. *Am J Hum Genet.* 2007; 81:1042–9. [PubMed: 17924344]
20. Sun B, Kulis MD, Young SP, Hobeika AC, Li S, Bird A, et al. Immunomodulatory gene therapy prevents antibody formation and lethal hypersensitivity reactions in murine pompe disease. *Mol Ther.* 2010; 18:353–60. [PubMed: 19690517]
21. Garnacho C, Dhimi R, Simone E, Dziubla T, Leferovich J, Schuchman EH, et al. Delivery of acid sphingomyelinase in normal and niemann-pick disease mice using intercellular adhesion molecule-1-targeted polymer nanocarriers. *J Pharmacol Exp Ther.* 2008; 325:400–8. [PubMed: 18287213]

22. Hsu J, Serrano D, Bhowmick T, Kumar K, Shen Y, Kuo YC, et al. Enhanced endothelial delivery and biochemical effects of alpha-galactosidase by ICAM-1-targeted nanocarriers for Fabry disease. *J Control Release*. 2011; 149:323–31. [PubMed: 21047542]
23. Muro S. New biotechnological and nanomedicine strategies for treatment of lysosomal storage disorders. *Wiley Interdiscip Rev Nanomed Nanobiotechnol*. 2010; 2:189–204. [PubMed: 20112244]
24. Muro S, Garnacho C, Champion JA, Leferovich J, Gajewski C, Schuchman EH, et al. Control of endothelial targeting and intracellular delivery of therapeutic enzymes by modulating the size and shape of ICAM-1-targeted carriers. *Mol Ther*. 2008; 16:1450–8. [PubMed: 18560419]
25. Muro S, Schuchman EH, Muzykantov VR. Lysosomal enzyme delivery by ICAM-1-targeted nanocarriers bypassing glycosylation- and clathrin-dependent endocytosis. *Mol Ther*. 2006; 13:135–41. [PubMed: 16153895]
26. Marlin SD, Springer TA. Purified intercellular adhesion molecule-1 (ICAM-1) is a ligand for lymphocyte function-associated antigen 1 (LFA-1). *Cell*. 1987; 51:813–9. [PubMed: 3315233]
27. Muro S. Intercellular Adhesion Molecule-I and Vascular Cell Adhesion Molecule-I. In: Aird, WC., editor. *Endothelial Biomedicine*. Cambridge University Press; 2007. p. 1058-70.
28. Muro S, Wiewrodt R, Thomas A, Koniaris L, Albelda SM, Muzykantov VR, et al. A novel endocytic pathway induced by clustering endothelial ICAM-1 or PECAM-1. *J Cell Sci*. 2003; 116:1599–609. [PubMed: 12640043]
29. Muro S, Cui X, Gajewski C, Murciano JC, Muzykantov VR, Koval M. Slow intracellular trafficking of catalase nanoparticles targeted to ICAM-1 protects endothelial cells from oxidative stress. *Am J Physiol Cell Physiol*. 2003; 285:C1339–47. [PubMed: 12878488]
30. Pagano RE, Puri V, Dominguez M, Marks DL. Membrane traffic in sphingolipid storage diseases. *Traffic*. 2000; 1:807–15. [PubMed: 11208071]
31. Parenti G, Andria G. *Pompe Disease: from New Views on Pathophysiology to Innovative Therapeutic Strategies*. *Curr Pharm Biotechnol*. 2011
32. Jevnikar AM, Wuthrich RP, Takei F, Xu HW, Brennan DC, Glimcher LH, et al. Differing regulation and function of ICAM-1 and class II antigens on renal tubular cells. *Kidney Int*. 1990; 38:417–25. [PubMed: 1977950]
33. Muro S, Dziubla T, Qiu W, Leferovich J, Cui X, Berk E, et al. Endothelial targeting of high-affinity multivalent polymer nanocarriers directed to intercellular adhesion molecule 1. *J Pharmacol Exp Ther*. 2006; 317:1161–9. [PubMed: 16505161]
34. Mundargi RC, Babu VR, Rangaswamy V, Patel P, Aminabhavi TM. Nano/micro technologies for delivering macromolecular therapeutics using poly(D, L-lactide-co-glycolide) and its derivatives. *J Control Release*. 2008; 125:193–209. [PubMed: 18083265]
35. Panyam J, Labhasetwar V. Biodegradable nanoparticles for drug and gene delivery to cells and tissue. *Adv Drug Deliv Rev*. 2003; 55:329–47. [PubMed: 12628320]
36. Broadhead DM, Butterworth J. alpha-Glucosidase in Pompe's disease. *J Inherit Metab Dis*. 1978; 1:153–4. [PubMed: 41974]
37. Hagemans ML, Stigter RL, van Capelle CI, van der Beek NA, Winkel LP, van Vliet L, et al. PAS-positive lymphocyte vacuoles can be used as diagnostic screening test for Pompe disease. *J Inherit Metab Dis*. 2010; 33:133–9. [PubMed: 20107902]
38. Bach G, Chen CS, Pagano RE. Elevated lysosomal pH in Mucopolidosis type IV cells. *Clin Chim Acta*. 1999; 280:173–9. [PubMed: 10090534]
39. Calderon AJ, Bhowmick T, Leferovich J, Burman B, Pichette B, Muzykantov V, et al. Optimizing endothelial targeting by modulating the antibody density and particle concentration of anti-ICAM coated carriers. *J Control Release*. 2011; 150:37–44. [PubMed: 21047540]
40. Schuchman, EH.; Desnick, RJ. Niemann-Pick Disease Types A and B: Acid Sphingomyelinase Deficiencies. In: Scriver, C.; Beaudet, A.; Sly, W.; Valle, D.; Childs, B.; Kinzler, K., et al., editors. *The Metabolic and Molecular Bases of Inherited Disease*. 8. Vol. 3. New York: McGraw-Hill; 2001. p. 3589-610.
41. Desnick, RJ.; Ioannou, YA.; Eng, CM. alpha-Galactosidase A Deficiency: Fabry Disease. In: Scriver, C.; Beaudet, A.; Sly, W.; Valle, D.; Childs, B.; Kinzler, K., et al., editors. *The Metabolic and Molecular Bases of Inherited Disease*. 8. Vol. 3. New York: McGraw-Hill; 2001. p. 3733-74.

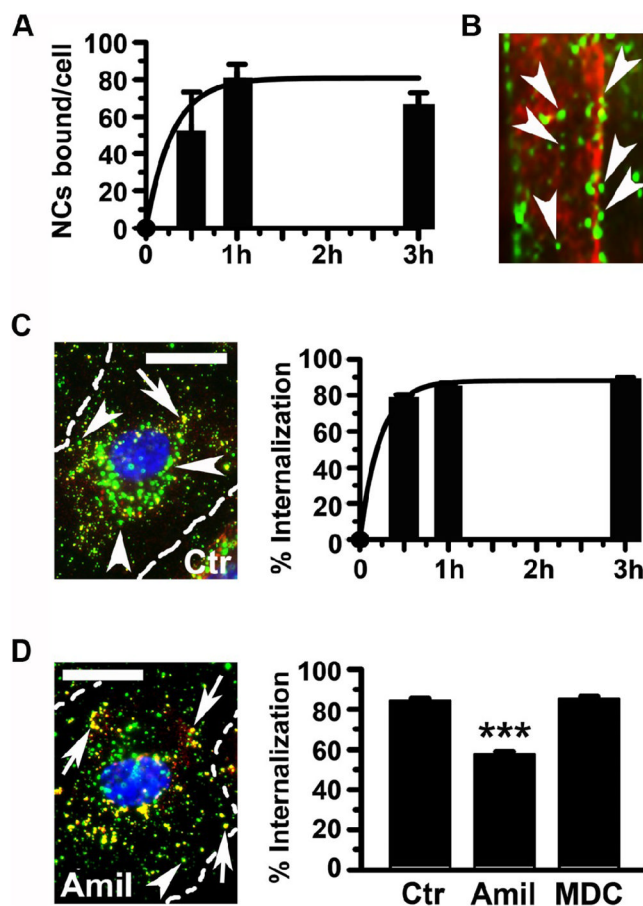


**Figure 1. Anti-ICAM/GAA NCs target and are internalized by Pompe-model cells via CAM endocytosis**

Binding of FITC-labeled anti-ICAM/GAA NCs to TNF- $\alpha$  activated, turanose-treated (A) HUVECs (30 min, 1 h, or 3 h, 37°C), analyzed by fluorescence microscopy, or (B) skeletal muscle cells from mice (5 h, 37°C), where arrowheads mark green carriers aligned on red-pseudocolored cytoskeletal fibers (from phase-contrast). (C–D) Micrographs (left; 1 h, 37°C) and quantification (right) of the internalization of FITC anti-ICAM/GAA NCs by HUVEC (30 min, 1 h, or 3 h, 37°C) in control media (C) or media containing amiloride to inhibit CAM endocytosis, or MDC to inhibit clathrin-coated pits. Surface bound nanocarriers were stained with Texas Red-labeled secondary antibody (double-labeled red + green yellow particles; arrows) versus internalized carriers (single-labeled green particles; arrowheads). Cell nuclei were stained with blue DAPI. Scale bar, 10  $\mu$ m. Data are mean  $\pm$ SEM (n = 32 cells, two experiments). \*\*\* $p$  0.001, by Student's  $t$ -test (compared to control cells).

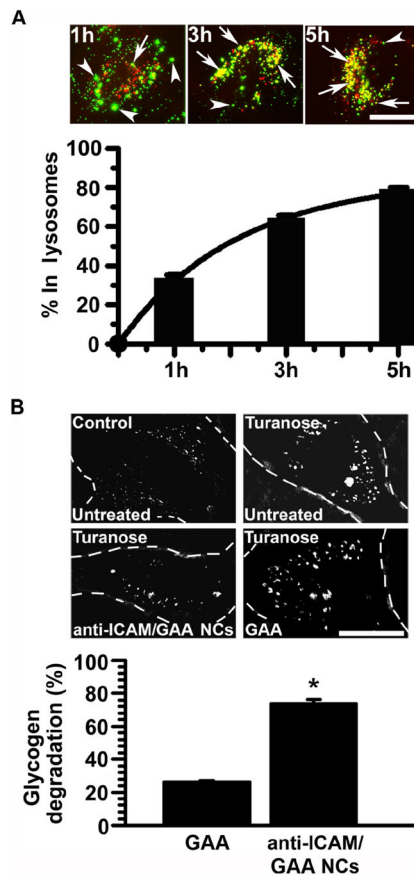


**Figure 2. Anti-ICAM/GAA NCs traffic to lysosomes and reduce glycogen storage in Pompe-model cells**

(A) FITC anti-ICAM/GAA NCs nanocarriers co-localizing with Texas-Red dextran-labeled lysosomes in Pompe disease-model cells are shown in yellow (red+green; arrowheads). Nanocarriers in other localizations are shown in green (arrows). Scale bar, 10  $\mu$ m. Data are mean $\pm$ SEM (n = 50 cells, two experiments). (B) Glycogen levels (determined by PAS staining) in cells treated for 5 h with a similar dose of neutral GAA coated on anti-ICAM NCs or as a free counterpart, in the presence of chloroquine, a base that inhibits the activity of endogenous acidic GAA but not exogenously administered neutral GAA. Data are mean  $\pm$ SEM (n = 49 cells). \* $p$  0.05, by Student's  $t$ -test (compared to untreated disease cells).

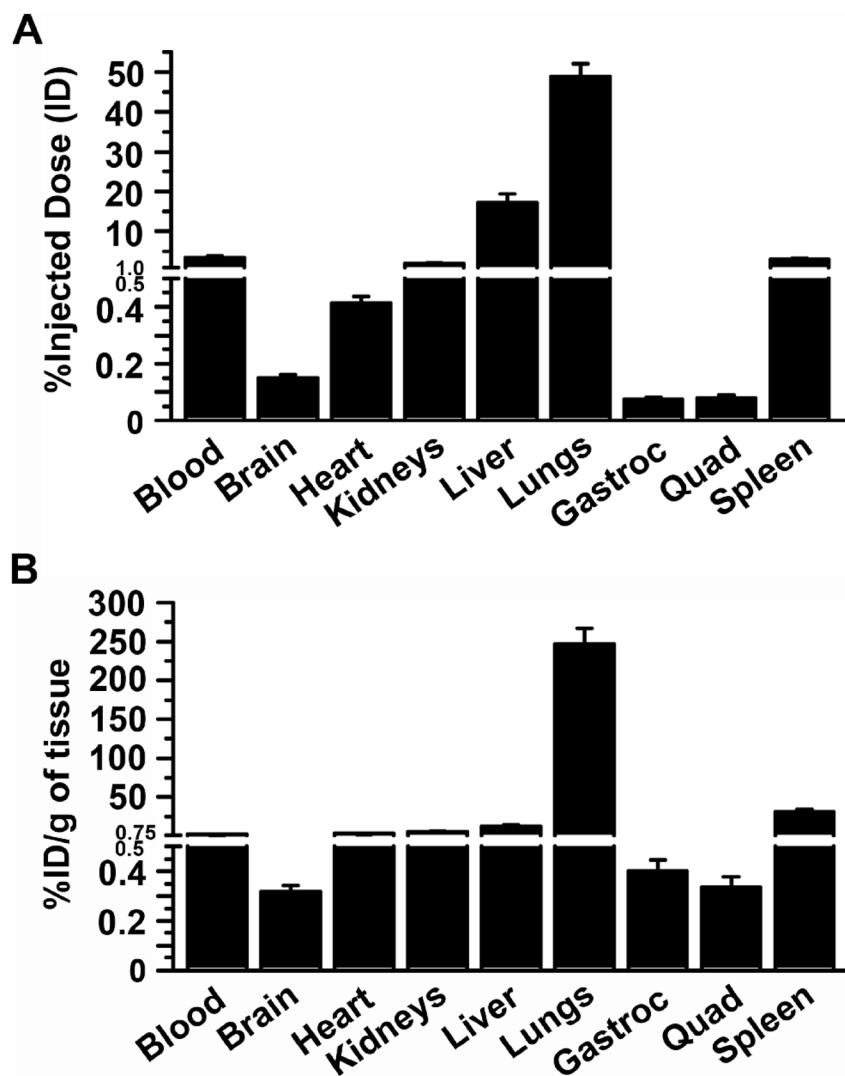


**Figure 3. Biodistribution of anti-ICAM/GAA NCs in mice**

Anti-ICAM/ $^{125}\text{I}$ -GAA NCs were injected intravenously in mice, and blood and organs were collected 30 min after injection. The samples were weighed and measured for  $^{125}\text{I}$ iodine content. (A) Percentage of injected dose (%ID) per organ was calculated to determine  $^{125}\text{I}$ -GAA in circulation and tissue accumulation. (B) Percentage of injected dose per gram of tissue (%ID/g) was calculated to compare  $^{125}\text{I}$ -GAA delivery among organs of different size. Gastroc = gastrocnemius. Quad = quadriceps. Data are mean $\pm$ SEM (n = 4 mice).

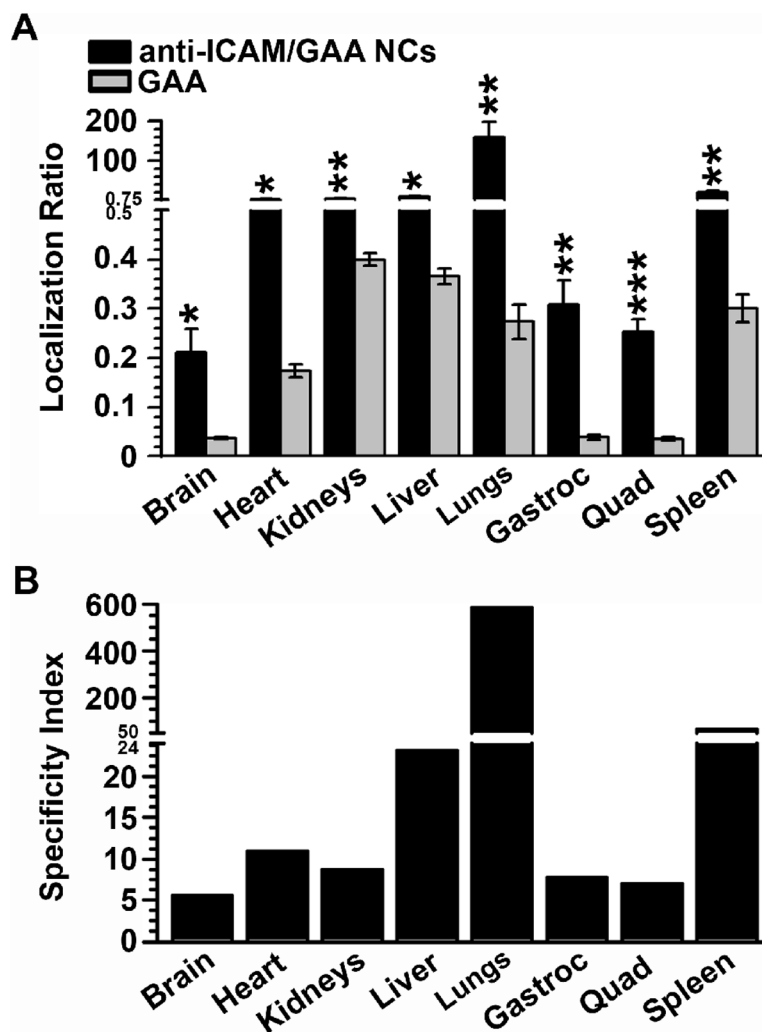


**Figure 4. Anti-ICAM NCs enhance delivery of GAA over non-targeted enzyme in mice** Anti-ICAM/ $^{125}\text{I}$ -GAA NCs or a similar dose of  $^{125}\text{I}$ -GAA were injected intravenously in mice, and blood and organs were collected 30 min after. The samples were weighed and measured for  $^{125}\text{I}$ iodine content. **(A)** The localization ratio (LR), calculated as percent injected dose per gram of organ (%ID/g) divided by %ID/g in blood, compares tissue accumulation for these two formulations with different circulation. **(B)** The specificity index (SI), calculated as the LR ratio of nanocarrier-targeted versus non-targeted  $^{125}\text{I}$ -GAA, reflects improved enzyme delivery of anti-ICAM NCs. Gastroc=gastrocnemius. Quad=quadriceps. Data are mean $\pm$ SEM (n = 3 mice). \* $p$  0.05, \*\* $p$  0.01, \*\*\* $p$  0.001, by Student's  $t$ -test (compared to free GAA).

**Table 1**

Load, transport and effects of ICAM-1-targeted nanocarriers for lysosomal delivery in cell culture.

	<b>Non- loaded</b>	<b>ASM</b>	<b><math>\alpha</math>-Gal</b>	<b>GAA</b>
Enzyme coating efficiency (%)	N/A	80	77	86
Enzyme molecule per NC (50:50 mass)	N/A	230	530	278
Anti-ICAM molecule per NC (50:50 mass)	250	135	138	123
Binding (NCs per cell)	165	160	70	80
% Internalization (1 h)	80	70	67	80
% Lysosomal transport (3 h)	75	70	70	65
% Lysosomal storage degradation (5 h)	N/A	98	70	75
Enhanced degradation (anti-ICAM/enzyme NCs: free enzyme)	N/A	2	2.5	3

N/A = not applicable. Data are mean values from this work and <sup>22,21,23,24</sup>.

**Table 2**

Biodistribution of ICAM-1-targeted nanocarriers for lysosomal enzyme delivery in mice.

	Blood		Brain		Heart		Kidney		Liver		Lung		Spleen	
	%ID	SI	%ID	SI	%ID	SI	%ID	SI	%ID	SI	%ID	SI	%ID	SI
Anti-ICAM NC	4.71 ± 0.94	0.19 ± 0.03	0.34 ± 0.04	1.34 ± 0.07	31.90 ± 3.58	26.35 ± 3.22	4.08 ± 0.48							
Anti-ICAM/ASM NC	6.94 ± 2.96	0.27 ± 0.05	7.24 ± 0.02	9.25 ± 0.05	39.60 ± 2.81	21.51 ± 2.73	4.08 ± 0.37	50.00						
Anti-ICAM/αGal NC	5.59 ± 0.33	0.13 ± 0.01	3.76 ± 0.04	5.06 ± 0.14	18.41 ± 1.22	36.24 ± 3.47	3.11 ± 0.43	52.94						
Anti-ICAM/GAA NC	3.32 ± 0.46	0.15 ± 0.01	5.56 ± 0.03	10.97 ± 0.18	17.32 ± 2.05	48.75 ± 3.25	2.91 ± 0.27	66.55						

%ID = percentage of injected dose. SI=specificity index (ratio of %ID/g of tissue to %ID/g of blood of the targeted strategy over the non-targeted enzyme). Data are mean±SEM, n = 4 mice (30 min after intravenous injection). Data are mean values from this work and 22,21,23,24.